JOURNAL OF AIRCRAFT
Vol. 47, No. 3, May–June 2010

Modeling Performance and Emissions from Aircraft for the Aviation Integrated Modelling Project

María Vera-Morales* and Cesare A. Hall†
University of Cambridge, Cambridge, England CB2 1PX, United Kingdom

DOI: 10.2514/1.44020

A new computational method has been developed that simulates the performance of a civil aircraft and determines the fuel consumption and emissions throughout the flight trajectory by linking the main aircraft aerodynamic characteristics with a model of engine performance. The performance emission simulation of aircraft operations model responds to the needs of the Aviation Integrated Modelling project by delivering a computationally fast and reliable model able to simulate aircraft performance, fuel use, and emissions. The methodology implies that the airframe aerodynamic characteristics and the performance of the engine are modeled by generic nondimensional relationships and related through the equations of motion. These nondimensional characteristics are sufficient to enable accurate determination of the forces acting on the aircraft, the fuel burn of the engine, and the key parameters that determine the emissions of pollutants such as nitrous oxides. Within this paper, this nondimensional approach is demonstrated and validated using comparisons with flight data from commercial aircraft operations. The results show that the model can accurately simulate civil aircraft performance for a range of flight conditions and operating procedures. In future work with the Aviation Integrated Modelling project, the method will be further developed and applied to investigate novel aircraft technologies, new operating procedures, and the use of alternative fuels.

Nomenclature

A_N	=	nozzle area (core and bypass), m^2
a_{long}	=	acceleration along the direction of flight, m/s^2
a_{nor}	=	acceleration perpendicular to the flight path, m/s^2
C_D	=	drag coefficient
C_L	=	lift coefficient
c_p	=	specific heat at constant pressure, kJ/(kgK)
D	=	drag, N
F_G	=	gross thrust, N
F_N	=	net thrust, N
g	=	acceleration due to gravity, m/s^2
L	=	lift, N
l	=	engine characteristic length, m
M	=	Mach number
$\dot{m}$	=	mass flow, kg/s
N_1	=	rotational speed of low-pressure shaft
P	=	pressure, Pa
P_a	=	atmospheric pressure, Pa
R	=	air gas constant, kJ/(kgK)
s	=	distance, m
T	=	temperature, K
T_a	=	atmospheric temperature, K
V	=	flight velocity, m/s
W	=	weight of the aircraft, N
α	=	angle of attack, deg
β	=	angle of climb/descent, deg
γ	=	ratio of specific heats
η	=	efficiency
π	=	generic nondimensional parameter
0	=	stagnation quantity
2	=	first compressor inlet
3	=	last compressor exit
4	=	turbine inlet
$\bar{}$	=	nondimensional

Subscripts

a	=	air
CR	=	cruise
f	=	fuel
is	=	isentropic
poly	=	polytropic

Presented as Paper 1263 at the 47th AIAA Aerospace Sciences Meeting, Orlando, FL, 5–8 January 2009; received 24 February 2009; revision received 4 February 2010; accepted for publication 9 February 2010.

*Postdoctoral Research Associate, Institute for the Aviation and the Environment, Engineering Department, Division A, Trumpington Street; mv234@cam.ac.uk.

†Lecturer in Turbomachinery, Institute for the Aviation and the Environment, Engineering Department, Division A, Whittle Laboratory, J. J. Thomson Avenue; cah1003@cam.ac.uk. Member AIAA.

I. Introduction

THE Aviation Integrated Modelling (AIM) project has the goal of developing a policy assessment tool for aviation, environment, and economic interactions at local and global levels, now and into the future. It contains a set of interlinked modules incorporating the key elements relevant to this goal (see Fig. 1). These include models for aircraft and engine technologies, air transport demand, airport activity, and airspace operations, all coupled to global climate, local environment, and economic impact blocks. This architecture of interacting modules is designed to capture major interdependencies and to enable environmental and economic tradeoffs to be examined. Further details of all the modules are given in [1].

Embedded within the AIM architecture, the Aircraft Technology Module aims to model the aircraft performance and emissions during all flight phases of any gate-to-gate flight operation of a commercial aircraft. The aircraft types to be modeled include current passenger airliners operating within the existing fleet as well as future aircraft that apply proposed airframe and engine technologies. The module is intended to accommodate various operational factors such as load factors, flight trajectories, and airline strategies, which are modeled by other modules within AIM. To enable rapid iteration with the other modules the module must be capable of rapidly simulating multiple aircraft flight trajectories across a network of routes.

There are several existing modeling tools capable of simulating aircraft flight profiles. Two of the models widely used by industry to simulate flight operations are the EUROCONTROL Base of Aircraft

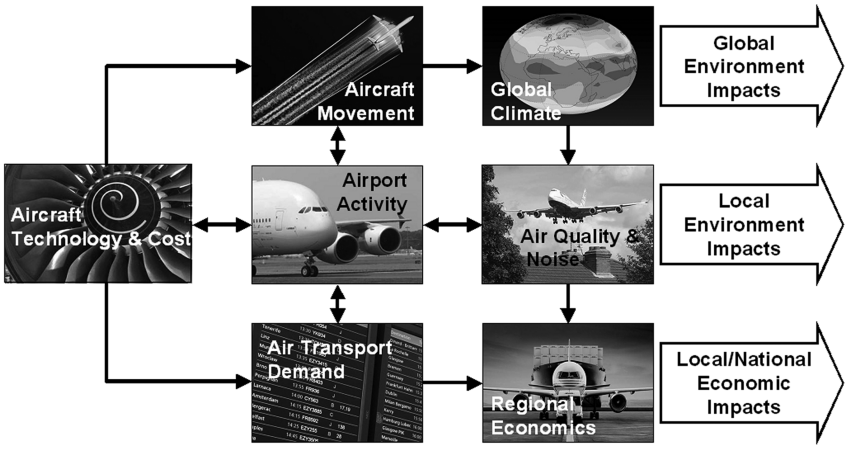

Fig. 1 Architecture of the AIM project [1].

Data (BADA) [2] and the PIANO aircraft analysis tool [3]. The former uses the principle of energy conservation combined with various performance and operating procedure coefficients for a large number of aircraft. These coefficients include those used to calculate thrust, drag, and fuel flow and those used to specify standard climb, cruise, and descent speed profiles. BADA has been found to be a reliable tool when standard flight procedures are simulated. This is expected, given that the required coefficients are derived from conventional airline operational procedures. However, the method is not applicable to nonstandard flight operations or novel aircraft technologies. In addition, the absence of a simulation of the thermodynamic cycle of the engine prevents combustion emissions from being calculated. PIANO is a commercial software package that makes use of very detailed aircraft aerodynamic characteristics but uses a relatively inflexible engine model. PIANO applies a dynamic model of the forces on the aircraft to determine the flight characteristics during different flight phases. This approach is found to be more accurate and flexible than that used by BADA, although it is also more demanding computationally.

This paper presents the method for simulating flight profiles that has been developed within the Aircraft Technology Module of the AIM project. The model is called PESO (Performance and Emission Simulation of Aircraft Operations) and its current version represents the first step toward meeting the needs of the Aircraft Technology Module. PESO has been designed to be fast and flexible yet still accurate enough to determine the impact of changes to technology and operational procedures on aircraft emissions. Within this paper, PESO results are compared with flight recorded data (FRD) for several flights of the Airbus-A320 aircraft. The comparisons show that PESO accurately reproduces the key features of the measured data for a wide range of flight operations for the mission legs of the flight corresponding to the climb to altitude and cruise phases. The study also shows that PESO can reproduce the absolute level of fuel consumption provided the airframe aerodynamic characteristics are accurately specified. However, some variability of the value of the lift-to-drag ratio L/D between similar flights of the same aircraft has been found in the flight recorded data. This could be partly due to the fact that the flight data used for the validation correspond to short haul flights. This implies that in order to calculate average flight trajectories in the context of AIM, a corresponding variability of the aerodynamic characteristic, L/D, should be also introduced.

The simplicity of the PESO methodology in combining a dynamic model of the airframe aerodynamics with a nondimensional model of the engine provides a computationally efficient method that includes sufficient detail to calculate emissions. The model has been developed using openly available data. Using the comparisons with FRD this paper makes a useful contribution to the field of aircraft simulation and it will be the basis of future aircraft emissions studies that will apply PESO to more complex scenarios.

II. Overview of the PESO Method

PESO simulates the performance of an aircraft and determines the fuel consumption and emissions at any point along the flight trajectory by linking the main aircraft aerodynamic characteristics with a model of engine performance. The method is based on the drag polar of the aircraft at cruise altitude and on a nondimensional representation of the engine.

Modeling the flight trajectory of an aircraft involves knowing the relation between the forces acting on the aircraft at each point of the flight mission. PESO considers the aircraft as a point mass and thus only the forces shown in Fig. 2 have to be taken into account.

The angle of attack (incidence) α is defined as the angle formed by the chord of the wing and the direction of the incoming flow. The angle of climb β is defined as the angle formed by the direction of the actual flight path and a plane horizontal to the surface of the earth. From Fig. 2, the generic equations governing the trajectory of the aircraft can be written as follows:

$$L(\alpha) + F_N \sin\alpha - W\cos\beta = a_{\text{nor}} W/g \tag{1}$$

$$-D(\alpha) + F_N \cos\alpha - W\sin\beta = a_{\text{long}} W/g \tag{2}$$

The dependency of the lift and drag on α and on the flight Mach number is presented in Sec. II.A. Considering these later dependencies, for a given weight of the aircraft and assuming that the acceleration in the direction perpendicular to the direction of flight, a_{nor}, is zero, the system of Eqs. (1) and (2), contains four unknowns (α, β, F_N, and a_{long}). To find a solution of the two equations, two of the variables should be fixed and hence the two remaining unknowns can be then calculated. For example, the angle of climb and the longitudinal acceleration are equal to zero at conventional constant level cruise. Therefore, the two remaining unknowns, F_N and α, can be calculated from Eqs. (1) and (2) using

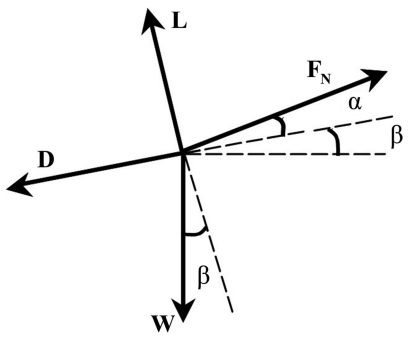

Fig. 2 Force balance for a point-mass airborne aircraft.

the relationships presented in Sec. II.A. Alternatively, the code can also be used as an optimizer to determine a combination of the four unknowns that meets a given target. Once the solution has been calculated, the fuel consumption can be determined from the net thrust in order to update the weight of the aircraft for the next trajectory point. For a given net thrust, the fuel consumption varies with flight speed and altitude. The modeling of the engine performance for each possible operating condition is presented in Sec. II.B and the procedure to run the model, i.e., the selection of the two variables to be fixed at each phase of the flight, is presented in Sec. II.C. Finally, the calculation of the pollutant emissions is presented in Sec. II.D.

A. Airframe Aerodynamics

To solve Eqs. (1) and (2), the dependency of the lift and drag on the angle of attack should be specified. The relationship between the lift and the drag is conventionally given as the lift-to-drag ratio L/D as a function of the lift coefficient C_L. Figure 3 shows an example of such representation for an Airbus-A320 aircraft taken from [3] at a conventional cruise altitude and for a range of flight Mach numbers. In the current version of PESO these data are used as input to the model throughout the entire flight mission. The effect of Reynolds number on the drag polars has been considered by modifying the zero-lift drag coefficient according to the Karman–Schoenherr correlation presented in [4]. The latter is based on the skin-friction drag coefficient due to a fully turbulent flow past a flat plate as a function of the Reynolds number. The effect of the Mach number on the drag polar is obtained from the data presented in Fig. 3, in which the compressibility effects are considered by using small variations of the Mach number and lift coefficient from a nominal optimum operating point just below the drag divergence Mach number. However, nonlinear variations of the drag are expected when the Mach number increases above the later value due to the transonic wave drag. This effect, not modeled here, is likely to be found for the higher cruise Mach numbers.

The second relationship required to solve Eqs. (1) and (2) is the one between the lift coefficient and the angle of attack. To determine this dependency it has been assumed that the two variables are proportional over the range of conventional angles of attack used for civil aircraft operations. The constant of proportionality has been estimated by using the approach presented in [5] which makes use of the wing sweep angle and aspect ratio in addition to the freestream Mach number to calculate the lift slope.

High-lift devices are required to create further lift at certain phases of the flight (typically takeoff, initial climb, approach, and landing). In the current paper, only the clean aircraft configuration, i.e., with the high-lift devices retracted, will be presented. Some of the limitations of this approximation are considered later in the paper.

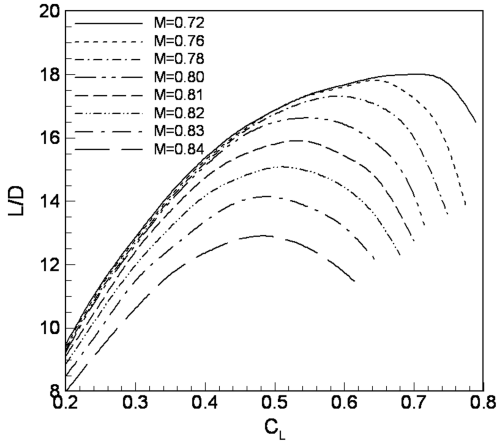

Fig. 3 Typical variation of L/D with C_L and Mach number for a passenger aircraft at conventional cruise altitude, derived from data given in [3].

B. Engine Modeling

In the analysis presented in this paper only turbofan engines are considered. To accurately model the engine at each point of the trajectory, its performance should be simulated for every possible operating condition, i.e., for each altitude, flight Mach number, and fuel flow rate to the engine. If each of these possible combinations had to be considered, a large number of calculations would be required. This complexity can be overcome by using a set of nondimensional engine performance parameters. The full derivation of the appropriate nondimensional parameters is out of the scope of this paper and can be found in [6] and in [7]. In this paper, only the main assumptions will be mentioned in order to understand the applicability and limitations of the method.

For the analysis presented here it is assumed that the Reynolds number is high and the angle of attack is small so that minor variations do not affect the performance of the engine. Under these assumptions the engine is affected only by the atmospheric conditions, the flight Mach number, and the fuel flow to the engines. Of all of these, only the fuel flow can be considered as a control variable. If it is assumed that the final nozzles (core and bypass) are choked, then the operating condition of the engine is independent of the static pressure downstream of the nozzle throat (approximately the atmospheric pressure). Hence, any engine performance parameter can be written as a function of the fuel flow and the inlet stagnation pressure and temperature: $\dot{m}_f$, P_{02} and T_{02} respectively. Starting from these variables, a nondimensional parameter can be formed, and hence any generic nondimensional parameter $\bar{\pi}$ can be written as

$$\bar{\pi} = f(\bar{\dot{m}}_f = \dot{m}_f \mathrm{LCV}/(P_{02} l^2 \sqrt{C_p T_{02}})) \tag{3}$$

where LCV is the lower calorific value of the fuel (generic kerosene). The conventional nondimensional parameters for the air mass flow, rotational speed and temperature, and overall pressure ratios are as follows:

$$\bar{\dot{m}}_a = \frac{\dot{m}_a \sqrt{C_p T_{02}}}{l^2 P_{02}}, \quad \bar{N}_1 = \frac{N_1 l}{\sqrt{\gamma R T_{02}}}, \quad \mathrm{TR} = \frac{T_{04}}{T_{02}}, \quad \mathrm{OPR} = \frac{P_{03}}{P_{02}} \tag{4}$$

where TR and OPR are the temperature ratio and overall pressure ratio, respectively. P_{02} is calculated assuming an inlet pressure recovery factor of about 99%, which is a reasonable assumption for podded mounted turbofans [8]. Each of the nondimensional parameters presented in (3) and (4) can be written as a unique function of any of the other parameters. As shown in [7], the appropriate nondimensional parameter associated with engine thrust is as follows:

$$\bar{F}_G = \frac{F_G + P_a A_N}{l^2 P_{02}} \tag{5}$$

Within PESO the net thrust and the thrust specific fuel consumption (sfc) are required at each point of the flight trajectory. The dimensional specific fuel consumption and net thrust can be calculated by recombining the nondimensional parameters with the flight condition and the engine size. Considering $l^2 = A_N$, the calculations are as follows:

$$\begin{aligned} \frac{F_N}{P_{02} A_N} &= \frac{(F_G - \dot{m}_a V)}{P_{02} A_N} = \left[\left(\frac{F_G + P_a A_N}{A_N P_{02}} \right) - \frac{P_a}{P_{02}} \right] \\ &\quad - M \left(\frac{\dot{m}_a \sqrt{c_p T_{02}}}{A_N P_{02}} \right) \sqrt{(\gamma - 1) \frac{T_a}{T_{02}}} \\ &= \bar{F}_G - \frac{P_a}{P_{02}} - M \bar{\dot{m}}_a \sqrt{(\gamma - 1) \frac{T_a}{T_{02}}} \end{aligned} \tag{6}$$

$$\text{sfc} = \frac{\dot{m}_f}{F_N} = \frac{\sqrt{c_p T_{02}}}{\text{LCV}} \left(\frac{\dot{m}_f \text{LCV}}{p_{02} A_N \sqrt{c_p T_{02}}} \right) \Big/ \left(\frac{F_N}{P_{02} A_N} \right)$$
$$= \frac{\sqrt{c_p T_{02}}}{\text{LCV}} \bar{\dot{m}}_f \Big/ \left(\frac{F_N}{p_{02} A_N} \right) \tag{7}$$

The underlying principle of the method implies that the relationships between the different nondimensional parameters collapse onto a single working line that is independent of the flight altitude and Mach number. This is true provided the assumption that the final nozzles are choked holds. Using this approach, once the working line is known, if one of the engine nondimensional parameters can be calculated, then all the others can be found and recombined with the flight condition and engine size to calculate the dimensional values. This requires many fewer calculations to be run. In addition, results can be scaled to any engine that has the same technology level.

To calculate the relationship between the nondimensional parameters, a commercial gas turbine cycle analysis package called GasTurb is used [9]. Figure 4 shows typical results from GasTurb for a turbofan engine. Figure 4a is a carpet plot showing the variation of specific fuel consumption with the net thrust for different altitudes and Mach numbers. Figures 4a and 4b demonstrate the principle that the nondimensional fuel flow and thrust are related via a single working line that applies to all flight conditions. The entire carpet plot on Fig. 4a is replotted with the solid line and symbols labeled as Model in Fig. 4b.

Figures 5a and 5b show results from the same modeled turbofan engine along with flight recorder data presented in terms of the nondimensional parameters described above. These figures show that there is a single working line that relates each pair of nondimensional groups. For the engine model, the working line is calculated by throttling the engine at a given altitude and Mach number. To calculate the nondimensional parameters presented in the figure for the flight data, only raw measurements for a single flight have been used, i.e., no external estimates have been employed. The results presented in Fig. 5 show that if the core and bypass nozzles are choked, as is the case for the data with overall pressure ratios larger than 20, the real engine does indeed operate on a single working line with a similar trend to that predicted by the model. However, for the lower range of overall pressure ratios, the nozzles are no longer choked and the dependency of the engine parameters on the atmospheric pressure should be then considered in the model. It is worth stating that the larger discrepancy found between the nondimensional N_1 of the FRD and that of the model does not affect the performance of PESO, as N_1, when used in the model, is given as a percentage of the design N_1.

C. Operations

The PESO model is a flexible tool, since any flight operation can be modeled provided the engine is operating with the choked nozzles and the high-lift devices are stowed. Figure 6 shows a plot of altitude versus Mach number for a specific flight mission (FRD values) and for the corresponding PESO results during climb (cruise and descent

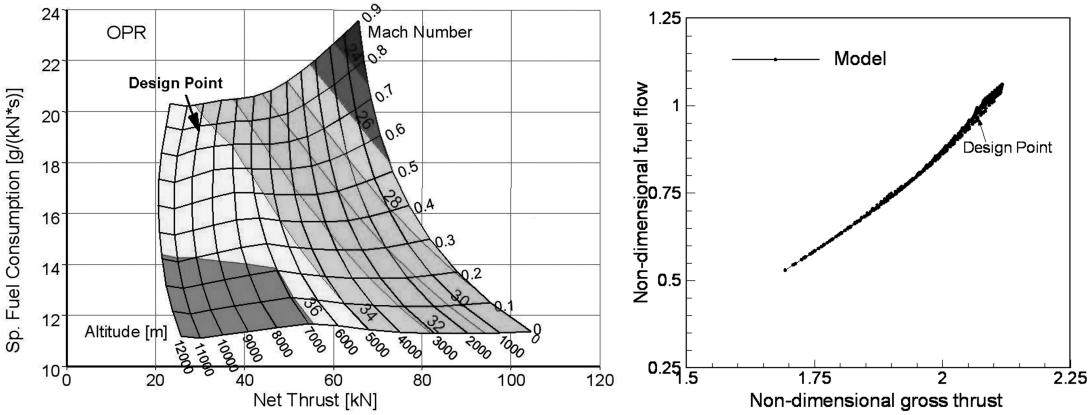

a) b)

Fig. 4 GASTURB model of an aircraft engine: a) variation of sfc with net thrust for different flight conditions and b) same data plotted in nondimensional form.

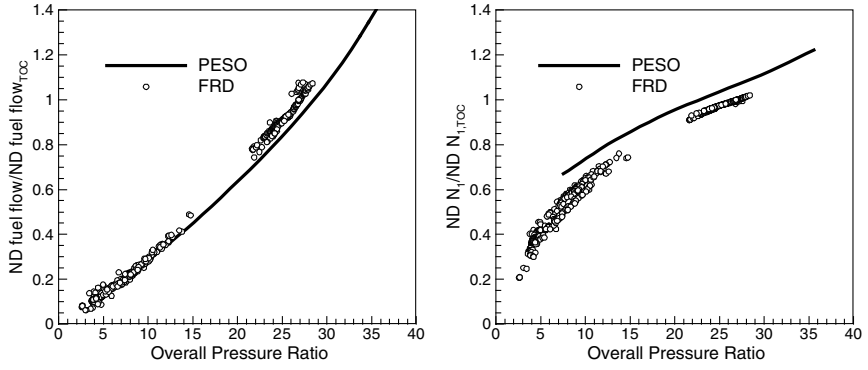

a) b)

Fig. 5 PESO nondimensional model of an aircraft engine compared with flight recorder data: a) variation of nondimensional fuel flow and b) nondimensional engine speed with OPR.

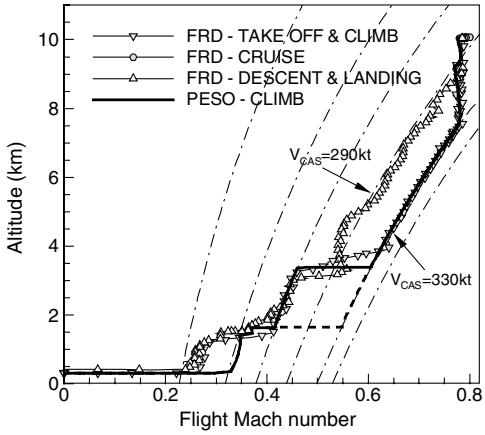

Fig. 6 Altitude versus Mach number for a conventional commercial flight during takeoff and climb.

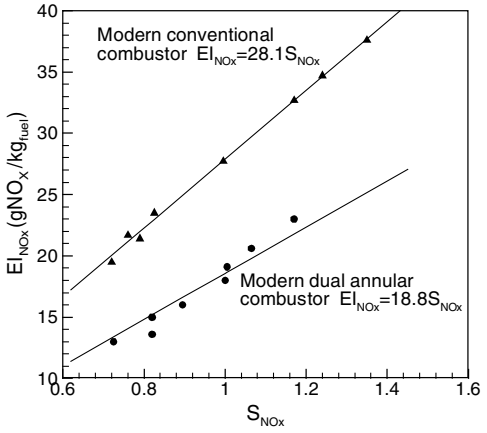

Fig. 7 Derivation of the combustor technology constant using the ICAO databank.

have been omitted for the sake of clarity). Lines of constant calibrated airspeed (CAS) are also shown in the figure as dashed-dotted lines.

For the climbing to top-of-climb (TOC), a standard operation procedure sets a high thrust setting (85–90% of N_1) and a profile of different calibrated airspeeds with altitude. In Fig. 6, the solid line represents the results from PESO when two different calibrated airspeeds are entered as a function of the altitude. If the input to the model is to be simplified and a generic profile is to be modeled, only one speed could be fixed, as shown by the dashed line in Fig. 6. These results demonstrate that fixing calibrated airspeeds is an effective way to ensure that PESO reproduces realistic climb trajectories. The effect of not including high-lift devices in the model can be seen in Fig. 6, in which the PESO results cannot reproduce the low-speed operation below an altitude of 1000 m. Note that in PESO, if the cruise Mach number is reached before TOC, the aircraft keeps ascending at constant Mach number.

In a conventional cruise phase the flight Mach number is held constant. In addition, if the cruise phase is flown at constant flight level, the angle of climb is set to zero; however, if there is an increase of flight level during the cruise phase, this is normally carried out at a constant angle of attack. For the descent, if a standard flight is to be simulated, the calibrated airspeed and angle of descent are fixed.

D. Emissions Modeling

Carbon dioxide, CO_2, has a long life span and its impact is independent of the location where it is released. More reactive pollutants (such as nitrogen oxides, NO_X) have a local as well as a global effect. The PESO model is able to provide the emissions from aircraft and the specific location where they were emitted. The subsequent impact of these emissions will be, in future work, determined by the Air Quality and Noise and the Global Climate modules in the AIM project (see Fig. 1). In this paper, the only emissions considered are CO_2 and NO_X. At a point i of the trajectory, the amount of a product of combustion emitted during a time interval δt is given by

$$p_i = (EI_p \cdot \mathrm{sfc} \cdot F_N)_i \cdot \delta t \tag{8}$$

where EI_p is the emission index of a generic pollutant p. By integrating expression (8) along the flight trajectory, the total amount of a pollutant emitted by the aircraft can be calculated. The emission index of a product of combustion depends on factors such as the composition of the fuel, the engine combustor technology, the engine temperatures and pressures, and the humidity of the air. For complete combustion of the fuel, the emission index of CO_2 depends solely on the mass fraction of carbon in the fuel. However, if the species is a nonstoichiometric product of combustion, the emission index can be determined from a severity factor S_{NO_X} that depends on the operating point of the engine. This severity factor for the case of NO_X, S_{NO_X}, is given in the following formula given in [10]:

$$EI_{NO_X} = C \cdot S_{NO_X} \tag{9}$$

where

$$S_{NO_X} = \left(\frac{P_{03}}{2965000}\right)^{0.4} \exp\left(\frac{T_{03} - 826}{194} + \frac{6.29 - 100\mathrm{war}}{53.2}\right)$$

where war is the water/air ratio (assumed to be zero here). The constant of proportionality, C, depends on the technology of the combustor and it can be calculated from the ICAO Aircraft Engine Emissions Databank [11], as shown in Fig. 7.

III. Validation

To validate PESO, the results from the model have been compared with flight recorder data for an Airbus A320 aircraft. These data include complete trajectory information as well as selected engine parameters. Although the accuracy of the fuel measurement varies with the actual fuel flow, worse at lower flow rates, the uncertainty is always less than 1% of the cruise fuel flow. PESO requires as inputs the drag polar of an A320, which has been derived from [3], and a GasTurb model of the appropriate engine. The engine, a two-shaft unmixed-flow turbofan, has been modeled from data available from CFM International.[‡]

The first part of the validation is presented in Sec. III.A, which compares the performance of the engine model with measurements from real engines. Section III.B compares aircraft fuel burn data from the FRD with predictions from PESO for flights with a constant-level-cruise phase. An evaluation of the results is then carried out for flights at various cruise altitudes, Mach numbers, and aircraft weights.

A. Engine Modeling

Figure 8 is a plot of nondimensional mass flow rate versus engine pressure ratio for a complete flight mission. The flight data presented have been divided in three groups according to the phase of the flight: 1) takeoff and climb, 2) cruise, and 3) descent and landing. The data corresponding to takeoff, climb, and cruise collapse onto a single line for pressure ratios in the range 20–30. During descent and approach the pressure ratio is lower than 15, due to the lower throttle setting during this phase, and there is a larger scatter of the data. This is expected, due to the unchoking of the final nozzles.

Figure 8 shows two engine working lines generated by GasTurb. The curve with the cross markers (engine 1) represents the performance expected for a two-spool unmixed-flow turbofan engine, similar to the one mounted on the aircraft, with standard component efficiencies (GasTurb default values). The design point of the engine is simulated by setting the general parameters given on

[‡]Data available online at http://www.cfm56.com/products/cfm56-5b/9662 [retrieved Sept. 2009].

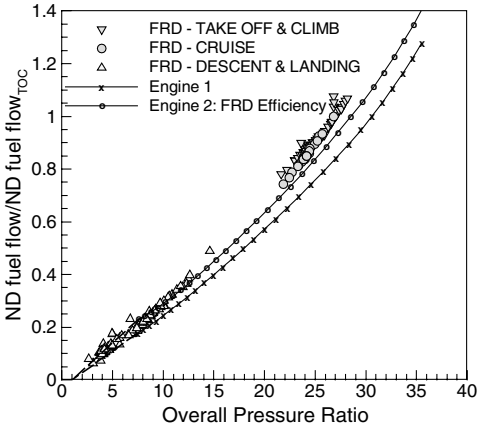

Fig. 8 Variation of nondimensional fuel flow with OPR for engine flight data and two engine models.

the manufacturer's Web page, such as the overall pressure ratio and the thrust at top-of-climb, as iteration targets for the calculation of the cycle. Conventional estimations of the turbine stator outlet temperature (see, for example, [7]) can be used to limit the exit temperature of the combustor and, moreover, the dimensions of the engine can be used to determine the bypass and fan pressure ratios. Once a design point is calculated, the operating line is calculated by changing the relative high-pressure spool speed.

The curve with the circle markers (engine 2) in Fig. 8 is a similar model of the engine that has been adjusted in trying to match the engine FRD. This adjustment has been made by considering the measurements of engine pressure and temperature included in the FRD. The stagnation pressure and stagnation temperature at the exit of the high-pressure compressor are included in the flight data, and it is thus possible to determine a polytropic efficiency for the combined low- and high-pressure compressors using the following equation:

$$\eta_{\text{poly}} = \left(\frac{\gamma - 1}{\gamma}\right) \cdot \frac{\ell_n(P_{03}/P_{02})}{\ell_n(T_{03}/T_{02})} \tag{10}$$

For the FRD flight profile presented in Fig. 8, the average value of the polytropic efficiency can be calculated and introduced as the input of the efficiency of the inner part of the fan and the core compressor. These values have been calculated using only the points corresponding to the legs of the mission in which the nozzle is choked and the high-lift devices are deployed. During descent, the engine is operating far from the design point and therefore a significant reduction of the polytropic efficiency is expected. To complete this model, the efficiencies of the high- and low-pressure turbines were varied, within the conventional range of the efficiency of the component, in an attempt to match the working line of the FRD engine. For this case, the entry temperature to the high-pressure turbine was increased to match the pressure ratio and maximum thrust of the original engine (engine 1). Figure 8 shows that the engine 2 model is in closer agreement with the FRD than the original engine model. There are still differences between engine 2 and the FRD, especially at high power settings. By increasing, for example, the amount of cooling flows to the nozzle guide vane and to the high-pressure turbine, the differences at high power settings could be reduced without much modification of the values at low power settings. However, for the sake of simplicity, only results from the more generic engine 2 model will be presented from here onward.

It is worth noting that in the context of AIM (Fig. 1), the age of the fleet could be taken into consideration by using a distribution of working lines with different component efficiencies to account for the engine in-service deterioration.

Note that the nondimensional models of the engines cannot be throttled down to the low overall pressure ratios that are characteristic of the engine operation during descent. To reach these values in the model, the working lines have been extended linearly from a pressure ratio of about 7 to a pressure ratio equal to 1, as shown in Fig. 8.

B. Constant Level Cruise

Figure 9 shows the fuel consumed during a constant level cruise of a typical A320 flight mission. At the end of cruise, the difference in fuel burn between the FRD and PESO run without any adjustments (labeled PESO in the figure) is about 75 kg of fuel. To investigate the origin of this difference in fuel burn, the values of L/D at which the aircraft is cruising have been investigated. For the PESO model, the value of L/D at each point of the profile is set by solving Eqs. (1) and (2) for a constant level cruise (angle of climb equal to zero) and a fixed cruise Mach number. For the cruise phase shown in Fig. 9, the average value of L/D calculated with PESO is about 17.8. For the flight data the value of the L/D at a point i of the constant-level-cruise trajectory for the flown distance Δs can be estimated from the Breguet–Range equation as follows:

$$\left.\frac{L}{D}\right|_i \cdot \frac{1}{\text{sfc}_i} = \frac{\Delta s \cdot g}{V_i\, \ell_n\left(\frac{W_{i+1}}{W_i}\right)} \tag{11}$$

where W_{i+1} and W_i refer to the weight of the aircraft at the beginning and at the end of Δs, respectively. The right-hand side term of Eq. (11) can be calculated directly from the flight data. The term with the specific fuel consumption on the left-hand side can be determined by combining the overall pressure ratio from the flight data with the engine model. Using this approach the average value of L/D for the cruise phase shown in Fig. 9 was found to be 19.3. The result of running PESO with a cruise L/D of 19.3 is also shown in the figure (labeled PESO + L/D_{FRD}), and by the end of the cruise, the difference in fuel consumed between this case and the flight data is negligible. Although an average L/D does not entirely determine the fuel consumed, i.e., the distribution of L/D along the flight leg also affects the performance, the results presented in Fig. 9 show that the methodology of the model is valid and that fuel burn data can be reproduced accurately provided the appropriate value lift-to-drag ratio is used.

Table 1 shows the effect of the altitude on the fuel consumed per kilometer during a constant altitude cruise for a given cruise Mach number and aircraft weight at top-of-climb. The weight of the aircraft has been nondimensionalized by the maximum takeoff weight (MTOW). A decrease in the fuel consumed with increasing altitude is captured by PESO, reflecting the lower fuel consumption of the engines at that higher altitude. However, the values of lift-to-drag ratio strongly influence the fuel burn, as can be seen in the comparison between PESO and the FRD at the lower-altitude case.

IV. Applications of PESO

The previous section presented a comparison between flight data and the corresponding results from PESO for a limited number of constant-level-cruise phases. This section investigates the capabilities of PESO for a wider range of flight operations. In Sec. IV.A variations in cruise fuel burn are presented for numerous cruise flight conditions. Sections IV.B and IV.C extend PESO to look

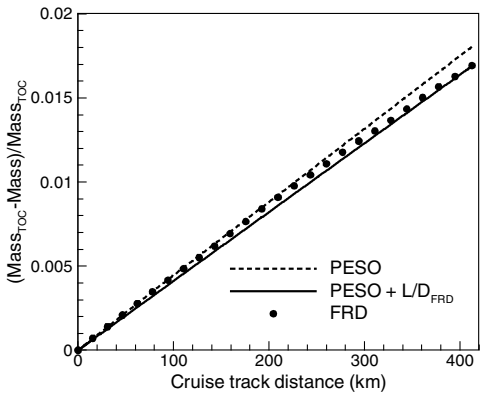

Fig. 9 Comparison between FRD and PESO at constant level cruise; altitude is 10,060 m and $M = 0.79$.

Table 1 Effect of the cruise altitude on the fuel burn and comparison between PESO and FRD[a]

	FRD		PESO	
Cruise altitude, m	9750 m	11890 m	9750 m	11890 m
Fuel burn, kg/km	3.51	2.37	2.69	2.36
L/D	13.0 (0.45)	18.3 (1.42)	16.9 (0.03)	17.8 (0.00)

[a]$M = 0.78$, $W_{\mathrm{TOC}}/\mathrm{MTOW} = 0.72$, and $s_{\mathrm{CR}} = 235$ km.

at aircraft performance during a stepped cruise and a full flight mission, respectively.

A. Constant Altitude Cruise

Figure 10 shows the fuel consumed per kilometer flown at cruise calculated by PESO for a given cruise length (600 km) as a function of Mach number (Fig. 10a), altitude (Fig. 10b), and mass of the aircraft at top-of-climb. In Fig. 10a, a minimum value of fuel burn is found, because for a steady level cruise at a given flight level, the ratio of the weight of the aircraft over the Mach number squared determines the value of C_L and the fuel burn. For a specific value of this ratio, the L/D is optimum. Similarly, as the flight level and the weight of the aircraft vary, so does C_L, leading to an optimum altitude. As expected, the results show that fuel consumption decreases as aircraft weight is reduced, confirming that nonpayload weight needs to be minimized in order to reduce emissions from aircraft. The increase in fuel consumption with an increase of the weight of the aircraft is due to the higher of angle of attack necessary to obtain the required higher lift. This brings about a larger drag (through the drag coefficient) and hence an associated increase of the thrust required from the engines.

B. Stepped Cruise

Standard cruise operations typically involve a stepped climb, especially during long cruise phases. Figure 11 shows a comparison between flight data including a stepped cruise and the corresponding result obtained with PESO. The trajectory of the flight data was matched with PESO (Fig. 11a) in order to compare the nondimensional fuel flow (Fig. 11b). The nondimensional fuel flow calculated from PESO shows the same trends as the flight data. These include a decreasing value during the portions of the flight at constant altitude due to the decreasing weight of the aircraft and the sudden increase due to the climb to the next flight level. It is worth noting that the fuel consumption decreases after the climb, but the larger decrease of atmospheric pressure and temperature increases the value of the nondimensional fuel flow at the higher-altitude segment. The magnitude of the step in the nondimensional fuel flow is also captured correctly by the model. This climb is normally flown at a constant angle of attack, ideally corresponding to the maximum L/D for a given Mach number. In Fig. 11, the cruise climb has been modeled by fixing a constant angle of attack, and although it does not affect the results significantly, it does determine the shape of the nondimensional flow curve during the climb.

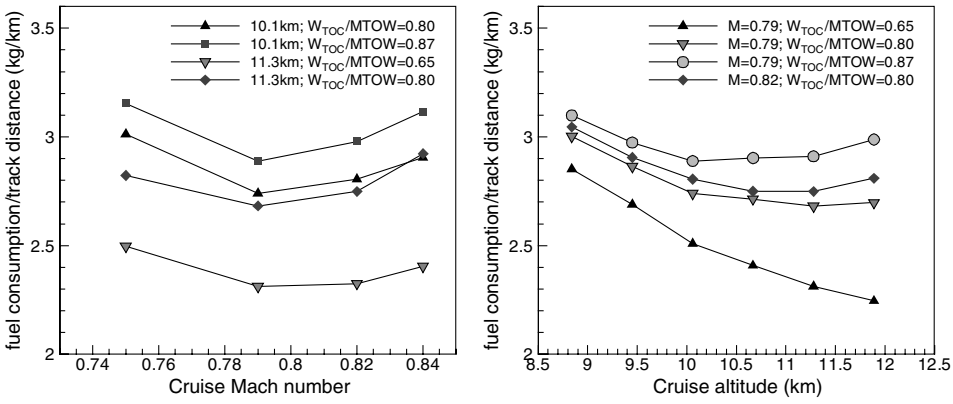

a) b)

Fig. 10 PESO fuel consumption per kilometer as a function of cruise Mach number, flight level, and aircraft weight at top-of-climb for a cruise-stage length of 600 km.

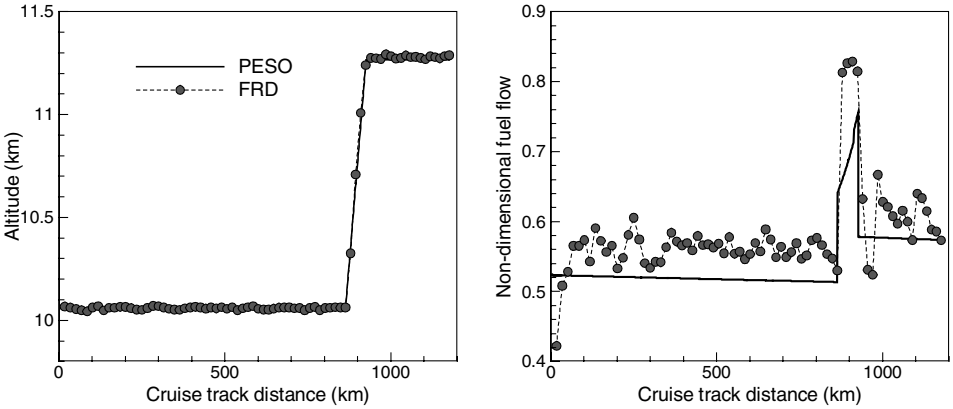

a) b)

Fig. 11 Comparison between FRD and PESO for a stepped cruise; $M = 0.78$.

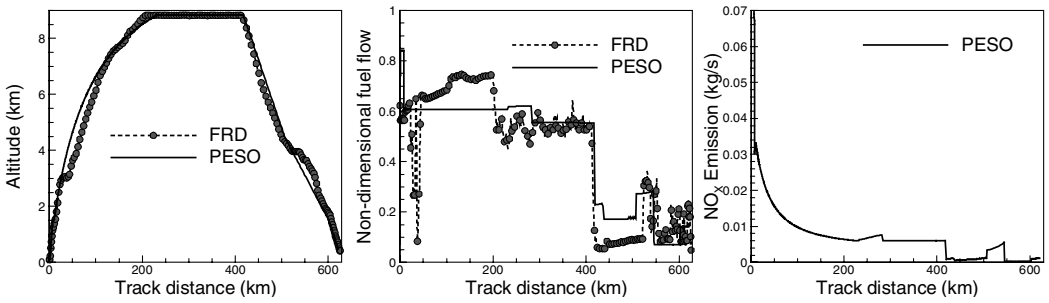

Fig. 12 Comparison between FRD and PESO for full flight mission.

C. Full Mission

The trends from PESO are compared with flight recorder data for a specific flight profile along the full flight mission (see Fig. 12). The flight trajectory (Fig. 12a) shows that PESO captures both the trend and the magnitude of the angle of climb along the climb phase with only the operation of the engine and the calibrated airspeed as inputs in Eqs. (1) and (2). Similar trajectories between both sets of data are also seen for the cruise and descent phases. Figure 12b shows the nondimensional fuel flow, and the right trends and levels are seen. The lower level of nondimensional fuel flow during climb calculated by PESO could be due, among other factors, to the lower fuel consumption of the modeled engine at high power settings, as seen in Fig. 8. Figure 12c shows the emission of NO_X (from the two engines) in kilograms per second for the specific flight under consideration assuming a modern dual annular combustor calculated using the methodology presented in Sec. II.D. The importance of an accurate modeling of the aircraft performance at takeoff is highlighted by the very high NO_X emissions, due to the high combustion temperatures, during this phase of the flight.

V. Conclusions

The performance and emission simulation of aircraft operations (PESO) model presented in this paper uses generic nondimensional relationships to describe the airframe and the engines in the modeling of aircraft trajectories. These nondimensional airframe and engine parameters are linked through the equations of motion. This methodology, based on publicly available data, has been validated using flight recorder data. The predictions of the different trends have shown that the methodology is sound, although the results are sensitive to the value of aircraft lift-to-drag ratio. The PESO model is a flexible tool that has been shown to be capable of reproducing a range of flight operations, including stepped cruise phases and complete flights. Aircraft with high-lift devices deployed need to be further investigated to improve the simulation of low-speed performance. In addition, now that the methodology has undergone some validation, in future work it could be applied to future aircraft technologies and new operating procedures.

Acknowledgments

The authors would like to thank Swiss Air for provision of the flight data presented. They would also like to acknowledge the financial support of the U.K. Engineering and Physical Sciences Research Council (EPSRC), the Natural Environment Research Council (NERC), and the Sir Arthur Marshall Institute for Aeronautics. Their support is gratefully acknowledged. Particular thanks are also due to past students, Noel Spillane and Hai Le, for their work on aircraft emissions modeling. The authors would like to thank Bill Dawes, colleagues from the Aviation Integrated Modelling (AIM) project, and the Institute for Aviation and the Environment at the University of Cambridge and at the Massachusetts Institute of Technology for the helpful discussions.

References

[1] Reynolds, T. G., Barrett, S., Dray, L. M., Evans, A. D., Köhler, M. O., Vera-Morales, M., et al., "Modelling Environmental & Economic Impacts of Aviation: Introducing the Aviation Integrated Modelling Project," Aviation Technology, Integration and Operations Conference, AIAA Paper 2007-7751, Sept. 2007.

[2] "User Manual for the Base of Aircraft Data (BADA)," Rev. 3.6, EUROCONTROL Experimental Centre, Brussels, 2004, http://www.eurocontrol.int/eec/gallery/content/public/document/eec/report/2004/022_BADA_User_Manual.pdf [retrieved Sept. 2009].

[3] *PIANO User's Guide* [online manual], Lissys, Ltd., Woodhouse Eaves, England, U.K., 2008, http://www.lissys.demon.co.uk/pug/index.html [retrieved Sept. 2009].

[4] Anderson, J. D., *Aircraft Performance and Design*, 1st ed., McGraw–Hill, New York, 1998, pp. 51–144.

[5] Küchemann, D., *The Aerodynamic Design of Aircraft*, 1st ed., Pergamon, Oxford, 1978, pp. 103–220.

[6] Hill, P., and Peterson, C., *Mechanics and Thermodynamics of Propulsion*, 2nd ed., Addison-Wesley, Reading, MA, 1992, pp. 196–202.

[7] Cumspty, N., *Jet Propulsion*, 1st ed., Cambridge Univ. Press, Cambridge, England, U.K., 1997, pp. 75–82.

[8] Anabtawi, A. J., Blackwelder, R. F., Lissaman, P. B. S., and Liebeck, R. H., "An Experimental Study of Vortex Generators in Boundary Layer Ingesting Diffusers with a Centerline Offset," 35th AIAA/ASME/SAE/ASEE Joint Propulsion Conference, AIAA Paper 99-2110, June 1999.

[9] GasTurb, Software Package, Ver. 11, Joachim Kurzke, 2004, http://www.gasturb.de [retrieved Sept. 2009].

[10] Gleason, C. C., and Bahr, D. W., "Experimental Clean Combustor Program: Phase III Final Report," NASA CR-135384, June 1979.

[11] *ICAO Aircraft Engine Emissions Databank* [online database], 2009, http://www.caa.co.uk/default.aspx?catid=702&pagetype=90, [retrieved Sept. 2009].